

Tuning the optical properties of 2D monolayer silver-bismuth bromide double perovskite by halide substitution

Original

Tuning the optical properties of 2D monolayer silver-bismuth bromide double perovskite by halide substitution / Schmitz, Fabian; Neisius, Raphael; Horn, Jonas; Sann, Joachim; Schlettwein, Derck; Gerhard, Marina; Gatti, Teresa. - In: NANOTECHNOLOGY. - ISSN 1361-6528. - 33:21(2022), p. 215706. [10.1088/1361-6528/ac54df]

Availability:

This version is available at: 11583/2975576 since: 2023-02-04T11:34:28Z

Publisher:

IOP

Published

DOI:10.1088/1361-6528/ac54df

Terms of use:

This article is made available under terms and conditions as specified in the corresponding bibliographic description in the repository

Publisher copyright

(Article begins on next page)

PAPER • OPEN ACCESS

Tuning the optical properties of 2D monolayer silver-bismuth bromide double perovskite by halide substitution

To cite this article: Fabian Schmitz *et al* 2022 *Nanotechnology* **33** 215706

View the [article online](#) for updates and enhancements.

You may also like

- [Perovskite-inspired materials for photovoltaics and beyond—from design to devices](#)
Yi-Teng Huang, Seán R Kavanagh, David O Scanlon *et al.*
- [Recent advances in lead-free double perovskites for x-ray and photodetection](#)
Joydip Ghosh, P J Sellin and P K Giri
- [Probing the charge transfer mechanisms in type-II Cs₂AgBiBr₆-CdSe composite system: ultrafast insights](#)
Gurpreet Kaur, Ayushi Shukla, Kaliyamoorthy Justice Babu *et al.*



Breath Biopsy® OMNI®

The most advanced, complete solution for global breath biomarker analysis

TRANSFORM YOUR
RESEARCH WORKFLOW



Expert Study Design
& Management



Robust Breath
Collection



Reliable Sample
Processing & Analysis





In-depth Data
Analysis



Specialist Data
Interpretation

Tuning the optical properties of 2D monolayer silver-bismuth bromide double perovskite by halide substitution

Fabian Schmitz^{1,2}, Raphael Neisius¹, Jonas Horn^{2,3}, Joachim Sann^{1,2}, Derck Schlettwein^{2,3} , Marina Gerhard^{4,*} and Teresa Gatti^{1,2,5,*} 

¹ Institute of Physical Chemistry, Justus Liebig University, Heinrich-Buff-Ring 17, 35392 Giessen, Germany

² Center for Materials Research, Justus Liebig University, Heinrich-Buff-Ring 17, 35392 Giessen, Germany

³ Institute of Applied Physics, Justus Liebig University, Heinrich Buff Ring 16, 35392 Giessen, Germany

⁴ Faculty of Physics and Materials Science Center, Philipps-Universität Marburg, Renthof 7a, Marburg D-35032, Germany

⁵ Centre of Excellence ENSEMBLE 3 sp. z o.o., Wolczynska 133, Warsaw, 01-919, Poland

E-mail: marina.gerhard@physik.uni-marburg.de and teresa.gatti@phys.chemie.uni-giessen.de

Received 17 December 2021, revised 4 February 2022

Accepted for publication 14 February 2022

Published 4 March 2022



Abstract

Silver-bismuth double perovskites are promising replacement materials for lead-based ones in photovoltaic (PV) devices due to the lower toxicity and enhanced stability to environmental factors. In addition, they might even be more suitable for indoor PV, due to the size of their bandgap better matching white LEDs emission. Unfortunately, their optoelectronic performance does not reach that of the lead-based counterparts, because of the indirect nature of the band gap and the high exciton binding energy. One strategy to improve the electronic properties is the dimensional reduction from the 3D to the 2D perovskite structure, which features a direct band gap, as it has been reported for 2D monolayer derivatives of $\text{Cs}_2\text{AgBiBr}_6$ obtained by substituting Cs^+ cations with bulky alkylammonium cations. However, a similar dimensional reduction also brings to a band gap opening, limiting light absorption in the visible. In this work, we report on the achievement of a bathochromic shift in the absorption features of a butylammonium-based silver-bismuth bromide monolayer double perovskite through doping with iodide and study the optical properties and stability of the resulting thin films in environmental conditions. These species might constitute the starting point to design future sustainable materials to implement as active components in indoor photovoltaic devices used to power the IoT.

Supplementary material for this article is available [online](#)

Keywords: silver-bismuth double perovskite, 2D perovskite, mixed-halide perovskite, lead-free perovskite

(Some figures may appear in colour only in the online journal)

1. Introduction

Lead halide perovskites received tremendous attention in the last decade due to their outstanding optoelectronic properties that make them suitable materials to be employed in the next generation of low-cost photovoltaic (PV) devices. However, the toxicity of the contained lead in combination with the

* Authors to whom any correspondence should be addressed.



Original content from this work may be used under the terms of the [Creative Commons Attribution 4.0 licence](#). Any further distribution of this work must maintain attribution to the author(s) and the title of the work, journal citation and DOI.

Table 1. Stoichiometric amounts of precursors used for the preparation of (BA)₄AgBiBr_{8-x}I_x (with $x = 0, 1, 2, 3, 4$) thin films.

Perovskite formula	AgBr (mg mmol ⁻¹)	AgI (mg mmol ⁻¹)	BiBr ₃ (mg mmol ⁻¹)	BiI ₃ (mg mmol ⁻¹)	C ₄ H ₁₂ NBr (mg mmol ⁻¹)
(BA) ₄ AgBiBr ₈	23.5/0.125	/	56.1/0.125	/	77.0/0.5
(BA) ₄ AgBiBr ₇ I	/	29.3/0.125	56.1/0.125	/	77.0/0.5
(BA) ₄ AgBiBr ₆ I ₂	/	29.3/0.125	37.2/0.08	24.8/0.04	77.0/0.5
(BA) ₄ AgBiBr ₅ I ₃	/	29.3/0.125	18.8/0.04	48.9/0.08	77.0/0.5
(BA) ₄ AgBiBr ₄ I ₄	/	29.3/0.125	/	73.7/0.125	77.0/0.5

limited stability against heat, moisture and air impede a broad commercialization [1]. In several approaches the substitution of Pb²⁺ was performed with other bivalent cations such as Sn²⁺ or Ge²⁺ to maintain the good optoelectronic properties by substitution with cations of similar electronic configuration [2, 3]. However, due to their preference of the oxidized states (Sn⁴⁺ or Ge⁴⁺) their environmental stability is further decreased. To expand the possible substitution options the usual bivalent cation was substituted with equal amounts of monovalent cations such as Cu⁺, Ag⁺ and Na⁺ and trivalent cations such as Bi³⁺, Sb³⁺ and In³⁺ [4, 5]. This approach forms a new perovskite class, known as double perovskite with the general formula A₂B⁺B³⁺X₆, which differ from the originated structure by the alternating occupation of the octahedral cavities with mono- and trivalent cations. Being these compounds generally characterized by higher band gaps compared to those of the bivalent perovskites due to preferential lattice stabilization as bromides, they might be more suitable to harvest the light coming from artificial lighting sources like white light emitting diodes (WLED) compared to the standard solar radiation, thus being suitable for use in indoor PV (optimum bandgap for indoor PV applications is in the range 1.9–2.0 eV, therefore far from the optimum one for outdoor that is between 1.1 and 1.4 eV) [6, 7].

Despite the high variety of prepared double perovskites, it has not been possible up to-now to reach the high optoelectronic performance of the lead-based ones. Several features of the 3D double perovskites limit their performance in optoelectronic devices, such as the indirect nature of their band gap, the high exciton binding energy and the low charge carrier lifetimes [8–10]. One possible approach to solve this issue is the dimensional reduction of the 3D bulk material towards the purely bidimensional form (precisely the monolayer one), which has been shown by calculations to provide direct band-gap species [11, 12]. To practically perform this structural modification, it is necessary to substitute the A⁺ cation in the 3D lattice with bulky primary ammonium cations, forming organic bilayers in between adjacent all-inorganic 2D planes in the so-called Ruddlesden–Popper phases [13–15]. However, together with a transition from an indirect to a direct bandgap, also an undesired bandgap opening takes place after production of the 2D monolayer double perovskites, which brings the material light absorption features in hypsochromic direction, thus also compromising possible use in indoor PV.

In this work we report on iodide doping [16–19] in a Ruddlesden–Popper 2D monolayer silver-bismuth bromide double perovskite featuring butylammonium cations as

organic spacers, named from now on with its formula (BA)₄AgBiBr₈, as a valuable strategy to achieve a red shift and broadening of the main absorption peak, which might make the resulting material more suitable for WLED light harvesting. We furthermore examine the structural properties and stability to prolonged illumination of the resulting thin films, trying to define the real potential of a similar low-toxicity material for use as active layer in indoor PV. While the formation of stable pure iodides for double perovskite structures has resulted elusive up to now [20], the mixing strategy might represent an alternative opportunity for the obtainment of comparable optical features, once the proper structural features for lattice stabilization have been identified.

2. Materials and methods

All the double perovskite precursors, namely BiBr₃ (99%), CsBr (99.9%), AgBr (99.5%) were purchased from Alfa Aesar. N-butylammonium bromide was purchased from Sigma Aldrich, as well as were the solvents. BiBr₃ was stored in a glovebox due to moisture sensitivity and AgBr in dark due to light sensitivity. AgI was synthesized by dissolving 1.447 g (8.518 mmol) of AgNO₃ and 1.418 g (8.542 mmol) of KI in 10 ml of demineralized water each, leaving the two resulting solutions to stir for 1 h at room temperature. Mixing of the two solutions led to precipitation of a yellow solid, that was filtered and dried at 120 °C in an oven over night. The obtained yellow powder was stored in the dark. BiI₃ was prepared by mixing solutions of Bi(NO₃)₃ · 5H₂O (1.656 g, 3.414 mmol) and KI (1.695 g, 10.21 mmol) in diluted HNO₃ (10 ml each). A black solid precipitated, which was filtered, washed with water and dried in oven at 120 °C.

2.1. Preparation of (BA)₄AgBiBr_{8-x}I_x (with $x = 0, 1, 2, 3, 4$) thin films

While in the past we employed an hydrothermal synthesis method to produce crystalline (BA)₄AgBiBr₈ and then with the resulting material we performed thin film fabrication through re-dissolution in dimethylformamide (DMF) [13], for the partial substitution of bromide ions in the metal-halide octahedra with iodides this method is not suitable, because it is normally conducted in excess of the halide (Br⁻ in this case) in hydrobromic acid solutions. Therefore, a solvent procedure was adopted, dissolving stoichiometric amounts of the AgBr, AgI, BiBr₃, BiI₃ and n-butylammonium bromide in DMF. The solvent procedure was first applied for the synthesis of

(BA)₄AgBiBr₈ to test its suitability to provide the pure compound directly in thin film form and then to synthesize the iodide-doped species. The amounts which are given in table 1 were weighed, dissolved in 500 μ l DMF and stirred overnight. All suspensions were heated up to 70 °C–80 °C to fully dissolve the precursors. In case of (BA)₄AgBiBr₅I₃ and (BA)₄AgBiBr₄I₄, which did not fully dissolve, 500 μ l and 1000 μ l of DMF respectively were added to complete the dissolution. These solutions varied in color from yellow to red-orange in relation to the dissolved iodide amounts, as shown in figure S1 (available online at stacks.iop.org/NANO/33/215706/mmedia) in the Supporting Information (S.I.). The solutions of the iodide doped double perovskite were directly used for thin film preparation on fluorine-doped tin oxide (FTO) transparent conductive substrates. The FTO-substrates were prepared by washing in an ultrasonic bath in demineralized water, ethanol and isopropanol for 5 min each. After drying, they were further cleaned for 15 min in an UV-Ozone Cleaner. The preparation of the thin films was performed in a glove box in an argon atmosphere by spin-coating. Therefore, the FTO-substrates were placed in the spin-coater and 35 μ l of the chosen perovskite solutions were added, followed by spin-coating at 4000 rpm for 40 s (acceleration of 200 rpm s⁻¹). Finally, the deposited films were heated at 100 °C for 4 min on a hotplate (also in the glovebox). Figure 1(b) shows the visual appearance of the obtained thin films for the different Br/I stoichiometries.

2.2. Characterization of (BA)₄AgBiBr_{8-x}I_x (with $x = 0, 1, 2, 3, 4$) thin films

UV–visible absorption measurements of thin films were carried out on an Agilent 8453 UV–vis spectrometer. Scanning electron microscopy (SEM) was performed on a Zeiss Merlin instrument at a working potential of 3 kV. Energy-dispersive x-ray (EDX) spectroscopy was performed on the same instrument at a working potential of 10 kV, an electron beam current of 3 nA and a X-Max 50 Silicon Drift Detector with 50 mm² active area and polymer window was used. Grazing incidence X-ray diffraction (GIXRD) was performed in a range of 3°–70° (0.05° step size, 0.014° s⁻¹ scan speed) with a PANalytical B.V. X'Pert Pro diffractometer using Cu K α 1 radiation. The diffraction patterns were measured along the 2 θ axis with a grazing incidence of $\omega = 0.5^\circ$. X-ray photoelectron spectroscopy (XPS) measurements were conducted with a PHI 5000 VersaProbe II Scanning ESCA Microprobe (Physical Electronics) with monochromatized Al K α X-ray source in high power mode (beam size 1300 μ m \times 100 μ m, X-ray power: 100 W). Time steps of 50 ms, a step size of 0.2 eV and an analyzer pass energy of 46.95 eV were used for measuring the detail spectra. The sample surface was charge neutralized with slow electrons and argon ions, and the pressure was in the range from 10⁻⁷ Pa to 10⁻⁶ Pa during the measurement. Data analysis was performed using the CasaXPS software [21]. Atomic force microscopy (AFM) and Kelvin probe force microscopy (KPFM) were carried out using an AIST NT Vacuscope 1000 microscope operated below 10⁻⁶ mbar with SPARK 350 Pt-coated AFM probes

excited at the resonant frequency of around 330 kHz. The work function was obtained by measuring the contact potential difference between probe and sample via FM-KPFM at an AC amplitude of 2 V at around 1 kHz. The probe work function was referenced by obtaining the contact potential difference of the probe to a freshly cleaved highly oriented pyrolytic graphite (ZYG, MikroMasch) with a known work function of 4.6 eV previous before and after each measurement. For time-resolved photoluminescence (TR-PL) spectroscopy, the samples were mounted in a microscopy cryostat (CryoVac) and cooled with liquid nitrogen. As excitation wavelength 380 nm was chosen, corresponding to the frequency-doubled output (760 nm) of a Titanium:Sapphire laser (Spectra Physics) with a repetition rate of 80 MHz and a pulse duration of ca. 100 fs. The average excitation power was approximately 1 mW. In order to suppress the excitation laser, several long-pass filters with a cut-off wavelength between 395 and 400 nm were placed in the detection path. The data was recorded with a synchroscan streak camera (Hamamatsu, C6860) and corrected by under-ground and spectral sensitivity of the detection system. Time-integrated PL spectra were obtained from the time-resolved streak camera data by summing up the intensity over all rows of the images. Note that the PL in all samples decayed almost entirely in the observed time window of 2 ns.

3. Results and discussion

The partial substitution of bromide ions with iodides within the metal halide octahedra of a perovskite structure to obtain mixed halide perovskites is a very common strategy to achieve a red shift of the absorption, due to the resulting bandgap reduction [22]. Unfortunately it is not always successful in providing pure mixed phases, but it often results in phase-segregation within thin films, providing domains of the sole bromide-rich phase separated by domains of the sole iodide-one [23, 24]. This phenomenon is not usually seen on freshly-prepared films, but can take place after exposure to light and/or other environmental factors. However, very recently it has been shown that, while in 3D perovskites this is a huge drawback for photo-active layers stability, in 2D perovskites the dimensional reduction might play a beneficial role in suppressing phase segregation [25, 26].

For this reason, we were prompted to attempt iodide substitution in previously reported lead-free (BA)₄AgBiBr₈ (figure 1(a)) [11, 13], a crystalline compound which was produced through hydrothermal synthesis, by mixing the inorganic bromide precursors and butylamine in hydrobromic acid solutions, and then re-dissolved in DMF to fabricate very homogeneous thin films via spin-coating. Unfortunately, a similar two-step procedure going through the hydrothermal product appeared unsuitable to the specific task that we were aiming at, namely the partial bromide substitution with iodide. This is due to the fact that the initial synthetic step is carried out in excess bromide ions (in concentrated aqueous HBr) and thus possibly compromising the incorporation of the iodide ions in the crystal lattice of the 2D double

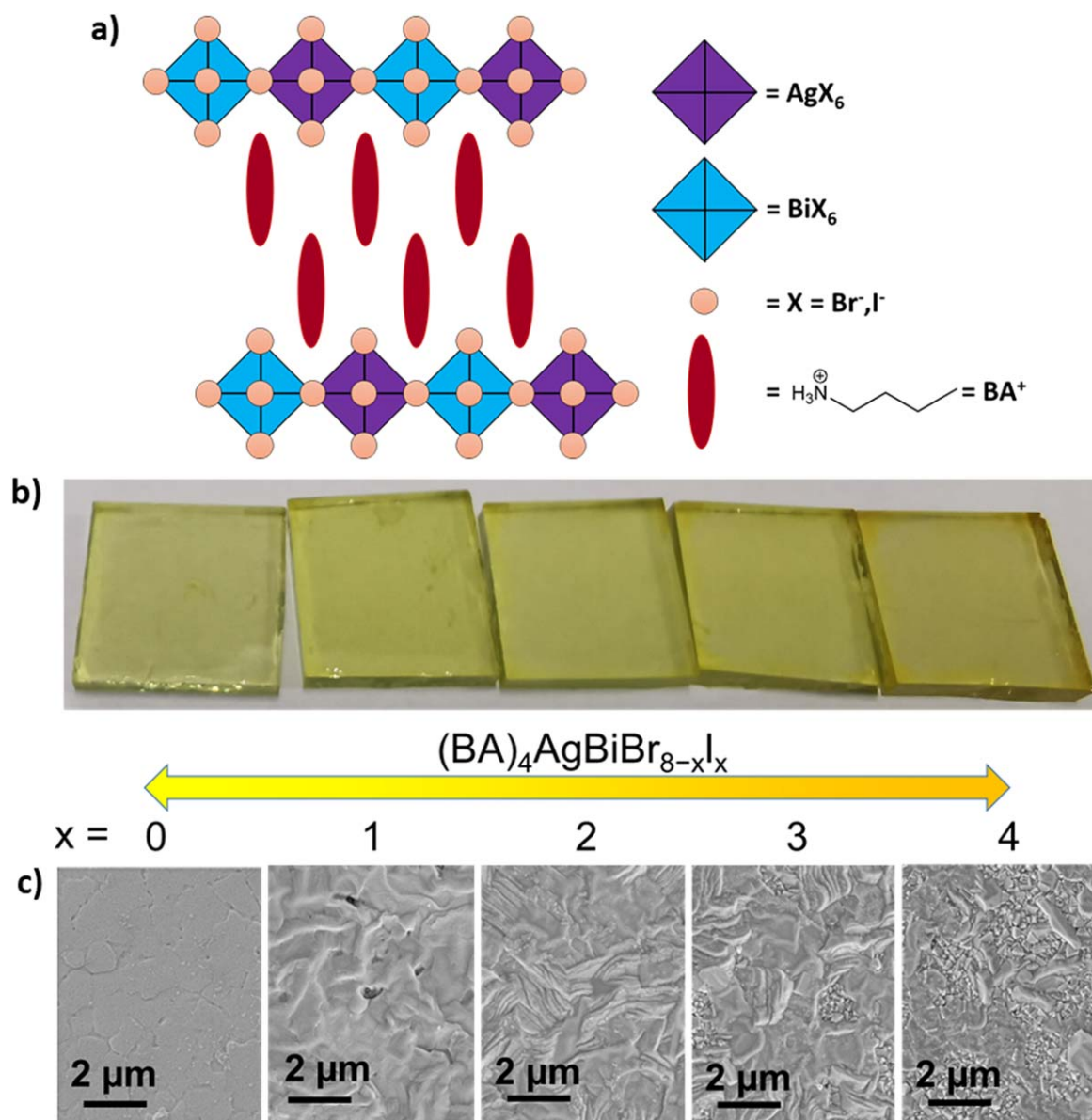


Figure 1. (a) Sketch of the structure of 2D monolayer silver-bismuth halide double perovskites of formula $(\text{BA})_4\text{AgBiBr}_{8-x}\text{I}_x$ (with $x = 0, 1, 2, 3, 4$) studied in this work. (b) Macroscopic aspect and (c) top-view SEM images of the resulting spin-coated thin films on FTO substrates.

perovskite. The preparation of two rare cases of pure iodides of 2D monolayers double perovskites was reported recently employing bifunctional ammonium cations (thus in a Dion-Jacobson conformation) [20, 27, 28], also operating in excess iodide in aqueous HI, but, to the best of our knowledge, no cases of mixed bromide/iodide of this type have been reported in the literature up to now. To be sure to introduce the right relative amount of the two halides in the mixed species, we chose to proceed through a one-step process starting from different relative stoichiometric amounts of AgI, BiBr_3 , BiI_3 and $\text{C}_4\text{H}_{12}\text{NBr}$ all dissolved in DMF and directly spin-coated on top transparent substrates to obtain thin films suitable for structural, optical and stability analysis (see details in the Materials and Methods section). In this way, we were able to prepare and study four different mixed bromide-iodide 2D-monolayer double perovskite samples, with increasing Br/I ratios, ranging from 7:1 to 6:2, 5:3 and 4:4.

However, given the limited solubility of BiI_3 in DMF, for the two highest iodide ratios we were forced to increase dilution in the precursor solutions, which resulted anyway darker than the others, already pre-announcing the possibility to achieve red-shift in the thin films prepared starting from them (see figure S1 in the S.I. for pictures of these solutions and figure 1(b) for that of the resulting films on FTO). On the other hand, all our attempts to prepare the pure iodide compound $(\text{BA})_4\text{AgBiI}_8$, both hydrothermally in concentrated aqueous HI and following the procedure for direct thin film preparation discussed before (with AgI, BiI_3 and $\text{C}_4\text{H}_{12}\text{NI}$ in DMF), failed. It might be possible that such a compound is unstable, as many other double perovskite iodides are [20].

The as-prepared thin films of $(\text{BA})_4\text{AgBiBr}_{8-x}\text{I}_x$ (with $x = 1, 2, 3, 4$) were studied through GIXRD and the resulting diffractograms were compared to that of a thin film of pure $(\text{BA})_4\text{AgBiBr}_8$ also prepared through the one-step procedure

(i.e. without previous preparation of the crystalline compound through hydrothermal synthesis), to probe the existence of one or more crystalline phases. The obtained GIXRD data for the thin films of $(\text{BA})_4\text{AgBiBr}_7\text{I}$, $(\text{BA})_4\text{AgBiBr}_6\text{I}_2$, $(\text{BA})_4\text{AgBiBr}_5\text{I}_3$ and $(\text{BA})_4\text{AgBiBr}_4\text{I}_4$ are reported in figure S2 of the S.I. At all the examined iodide contents, the GIXRD patterns of the $(\text{BA})_4\text{AgBiBr}_{1-x}\text{I}_x$ thin films show an intense (001)-reflex at almost 6.6° , which is nearly identical to that of the reference $(\text{BA})_4\text{AgBiBr}_8$ thin film (figure S1(a)). In samples with $x \geq 2$, another weak reflex at 13.2° appears, which is most likely the second order reflex of the (001) dominant scattering feature. For all compounds therefore, the crystalline phase is identical to that of $(\text{BA})_4\text{AgBiBr}_8$ and no side phases could be detected, allowing us to exclude the occurrence of phase-separation of an iodide-rich phase during the thin-film production process. However, by increasing bromide-iodide substitution, the shape of the dominant (001)-reflex becomes progressively broader, likely indicating the formation of smaller crystallites in the thin films (see figure S1(b)). In addition, since all reflexes are identified as (001)-reflexes or its multiples, an ordered layer structure parallel to the substrate is suggested.

The SEM images of the iodide-doped and reference $(\text{BA})_4\text{AgBiBr}_8$ thin films are reported in figure 1(c) (the macroscopic appearance of the same thin films as results to the naked eye is reported for the sake of clarity in figure 1(b), from which it can be noticed how the yellow color of the pure bromide reference becomes darker with increasing amounts of iodide substitution). While pure $(\text{BA})_4\text{AgBiBr}_8$ forms a very uniform and homogeneous film on the FTO substrate, the progressive increase in iodide content seems to affect the homogeneity of the layer. The microstructure of $(\text{BA})_4\text{AgBiBr}_7\text{I}$ reveals the presence of a layer mostly parallel to the substrate and with relatively good coverage of this last one, although in comparison with that of $(\text{BA})_4\text{AgBiBr}_8$ appears to be more disordered and featuring a few small pinholes. For $(\text{BA})_4\text{AgBiBr}_6\text{I}_2$ the SEM image shows an increased nano-structuring in the layer, as edges of packed layers are clearly visible. This trend in nano-structuring and reduced surface coverage continues with $(\text{BA})_4\text{AgBiBr}_5\text{I}_3$ and $(\text{BA})_4\text{AgBiBr}_4\text{I}_4$ and is further confirmed by AFM (see figure S6(a)). The reduced coverage of the substrate is most likely due to the higher dilution applied to the precursor solution for $(\text{BA})_4\text{AgBiBr}_5\text{I}_3$ and $(\text{BA})_4\text{AgBiBr}_4\text{I}_4$ due to the reduced DMF solubility of BiI_3 compared to that of BiBr_3 , as mentioned earlier. Such inhomogeneity prevented us from obtaining exact film thicknesses from SEM cross-sections. However, the film thicknesses of the thin films with high coverage ($x = 0, 1$) show values around 440 nm, while the thickness of the $x = 2$ film is significantly reduced to circa 100 nm, as can be inferred from figure S3.

To validate that the 2D monolayer double perovskite thin films have the same compositions that were given by the particular precursor solution composition, XPS analysis was performed, to compare the atomic ratios of Ag, Bi, Br and I, that can be calculated by their respective XPS spectra (see table S1 for a summary of all the calculated atomic ratios).

The XPS spectra in the Br and I region, reported in figures 2(a) and (b) respectively, show that the intensity of the

Br 3d spectrum decreases with increasing iodide substitution (here indicated as x) while the intensity of the I $3d_{5/2}$ spectrum increases with increasing x and shows no signal at $x = 0$, meaning that the reference $(\text{BA})_4\text{AgBiBr}_8$ perovskite contains no iodide as solely bromide precursors were used for its preparation (table 1). Furthermore, the direct comparison of the calculated bromide and iodide contents reported in figure 2(c) proves that the halide ratios match the corresponding precursor compositions. For what concerns the metallic components in the thin films, namely Bi and Ag, it is important to note that while the Bi 4f spectrum did only change slightly in intensity for any halide ratio (figure S5(b)) the intensity of the Ag 3d spectrum underwent larger changes across the different substitution stoichiometry, which cannot be anyway reconnected to the iodide-bromide ratio trends. In general, a Bi:Ag ratio of around 2:1 for each halide composition (see table S1) was detected, although equimolar amounts of Ag and Bi were used as precursors. These results are in agreement with our former evidences, indicating the presence of Ag-depleted regions in crystalline $(\text{BA})_4\text{AgBiBr}_8$ powder samples as resulted by EDX analysis carried out during transmission electron microscopy (TEM) imaging [13]. Additionally, we performed EDX measurements within the SEM to gain further insight into the bulk composition of the thin films, since XPS is a surface sensitive technique. However, due to the higher penetration depth of EDX with respect to XPS, only thick and homogeneous films ($x = 0, 1, 2$) provided reliable results on their atomic ratios (see table S2), while for the $x = 3, 4$ samples most of the signal could be assigned to the substrate. The calculated ratios of bromide and iodide which are plotted in figure S4 are in good accordance to the ratios calculated from the XPS measurements and the precursor ratios shown in table 1. Furthermore, elemental maps obtained from EDX, which are depicted in figure 6 (*vide infra*), show homogeneous distributions of bromide and iodide across the thin film for low iodide contents ($x = 1$) and only small inhomogeneities for increased iodide contents ($x = 2$).

The $(\text{BA})_4\text{AgBiBr}_{8-x}\text{I}_x$ thin films with progressively increasing substitution of bromide anions with iodide have been studied through UV-vis absorption spectroscopy to precisely evaluate the change in their optical absorbance. The resulting UV-vis spectra are reported in figure 3(a) and effectively demonstrate the progressive bathochromic shift of the optical absorption as a function of augmented iodide-bromide substitution. Since the film thickness and morphology is likely varying too, as we could detect from SEM, we normalized the spectra at their absorbance minimum in the area between 370 and 400 nm, to be able to compare relative variations in the peak intensities and shapes. The strong and relatively narrow peak with a maximum at 410 nm (~ 3 eV) in the pure bromide thin film is consistent with what was observed previously by us and by other authors [11, 13]. This transition is of apparent excitonic type and has been reported to feature a large contribution of the light-triggered charge transfer from Ag-d to Bi-s/Bi-p orbitals. Still, its exact nature, particularly in a highly confined space as that of a 2D monolayer structure, is subject of debate and it is well far

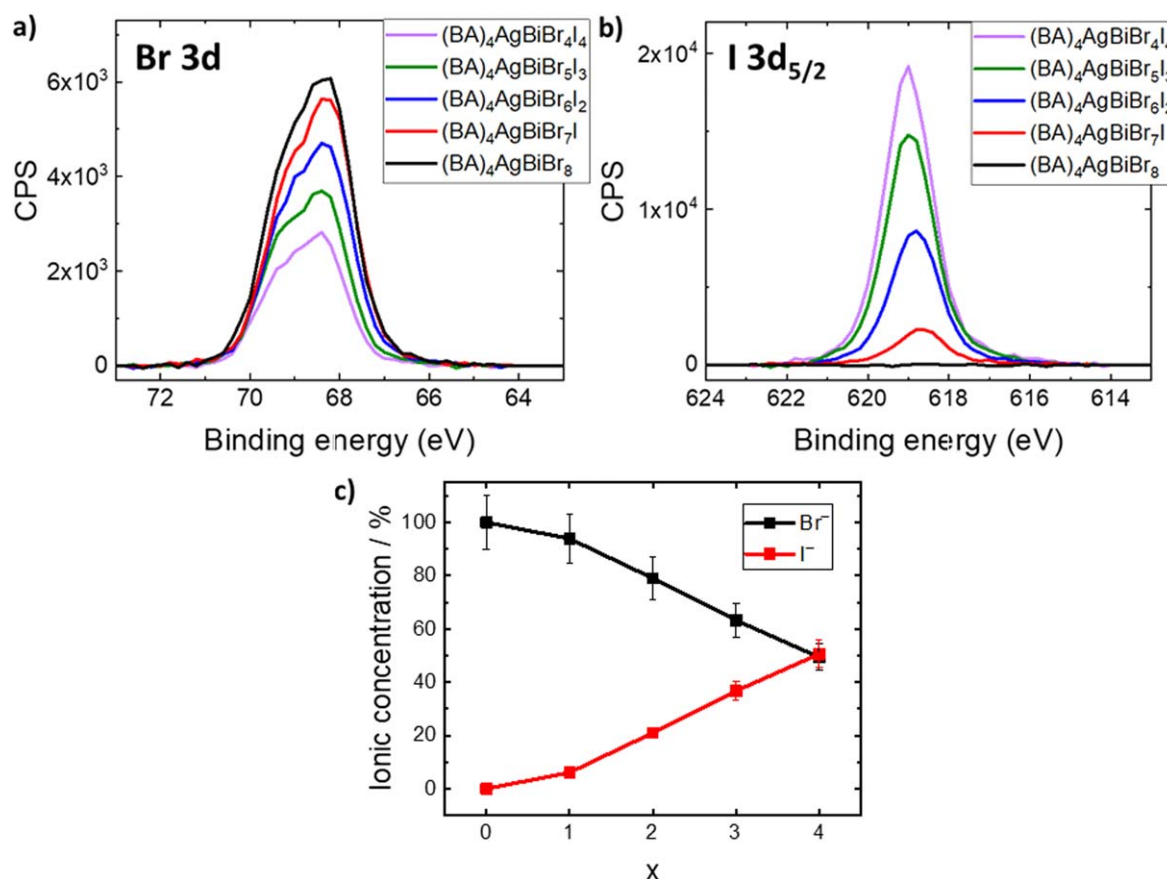


Figure 2. Details of the XPS spectra of the $(\text{BA})_4\text{AgBiBr}_{8-x}\text{I}_x$ ($x = 0, 1, 2, 3, 4$) thin films: (a) Br 3d region and (b) I 3d_{5/2} region. (c) Halide ions ratio variation in the corresponding films (the error bars include a relative error of 10% for each estimated concentration value).

from our intentions to provide a full explanation for it in the present work. What anyway appears to be perfectly clear is that by increasing the alloying percentage with iodide, this peak decreases in intensity, broadens and shifts its maximum towards longer wavelengths [up to 454 nm (~ 2.7 eV)] in the species with the highest iodide/bromide ratio, namely $(\text{BA})_4\text{AgBiBr}_4\text{I}_4$, as desired.

This shift might result from the partial participation of iodide atoms orbitals to the states involved in the edge optical transition, or to changes in the lattice constant following partial bromide replacement with iodide, this also perhaps related to a different orientation of the octahedra in the inorganic sheets in comparison to the situation in the pure $(\text{BA})_4\text{AgBiBr}_8$ [11]. The beneficial effect of iodide substitution on the band edge absorption bathochromic shifting is therefore well proven from these measurements. Still, the nature of the involved transitions and the reason for peak broadening are difficult to determine: very recently, Kanatzidis and coworkers reported for pure iodide 2D monolayer Ag–Bi double perovskites with small cyclic diammonium cations that an electronic transition from I-5p states in the valence band maximum to I-5p/ Bi-6p states in the conduction band minimum could better explain band edge absorption, when iodide is involved as the halide in this type of compounds [27]. Unfortunately, the absorption spectra of thin films of these compounds are not reported in their work, but only the Kubelka–Munk transformations applied on the diffuse reflectance spectra of the powder species, not allowing

a good comparison of the shape of this absorption with that measured for the here reported films. Nevertheless, it appears that also in their materials a rather broad absorption without pronounced exciton resonance characterizes the band edge features, as it is in the present case. Whether this broadening is a sign of decreased exciton confinement in these iodide-enriched materials [15, 29], is hard to clarify at this stage and remains subject of future investigations: what we can anticipate here is that, if this would be the case, it might have a beneficial effect on the charge transport properties that could favor photocurrent generation in suitable light-conversion architectures.

The optoelectronic properties of the mixed iodide-bromide 2D monolayer silver-bismuth double perovskite thin films have been further studied by PL spectroscopy. The room-temperature PL spectra of the thin-films obtained from laser excitation at 380 nm (~ 3.26 eV) are reported in figure 3(b). In earlier work, we have identified this excitation energy as the one giving the highest PL response for the reference $(\text{BA})_4\text{AgBiBr}_8$ material [13]. Moreover, as demonstrated in figure 3(a), this energy provides excitation well above the band gap for all investigated samples. The PL response of the pure bromide thin film confirms previous observations [11, 13], i.e. a relatively broad and weak emission centered at around 470 nm is recorded, likely due to a trap-assisted radiative recombination. In the present case, this emission appears also perhaps broader (larger full weight half maximum) than in precedent reports, featuring a tail which could derive from a self-trapped exciton

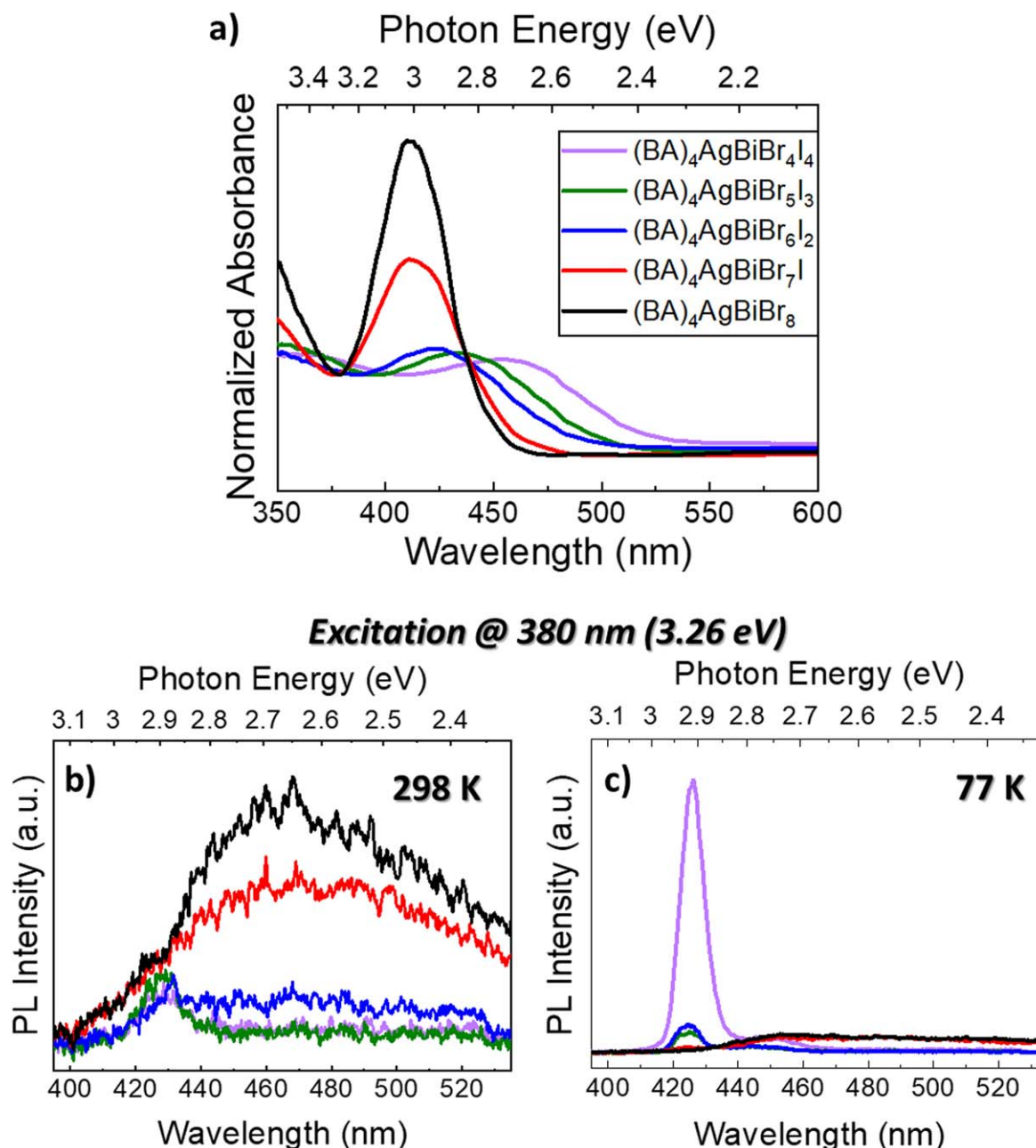


Figure 3. Optical properties of the $(\text{BA})_4\text{AgBiBr}_{8-x}\text{I}_x$ ($x = 0, 1, 2, 3, 4$) thin films: (a) UV–visible absorption and PL spectra measured at (b) room temperature (298 K) and (c) at 77 K ($\lambda_{\text{exc}} = 380 \text{ nm}$, $E_{\text{exc}} = 3.26 \text{ eV}$). The color/sample legend is reported only in the first graph for the sake of clarity.

(STE) contribution [30], by us seen up to now in a well-defined manner only for an isomeric compound in which the n-butyl ammonium cations were completely replaced by iso-butylammonium in the 2D monolayer double perovskite lattice [13]. The effect of iodide-bromide substitution on the PL behavior of the thin films is peculiar and points out at possible re-adjustments of the lattice, which however do not apparently affect the spacing between the 2D layers but mostly the inorganic nanosheets conformation, as we could not detect them through GIXRD (figure S2). The broad trap-mediated PL of the $(\text{BA})_4\text{AgBiBr}_8$ thin film progressively decreases and, in the samples with higher iodine content, namely $(\text{BA})_4\text{AgBiBr}_5\text{I}_3$ and $(\text{BA})_4\text{AgBiBr}_4\text{I}_4$, a new feature emerges at shorter

wavelength/higher energies (around 425 nm/2.9 eV), which is very narrow (linewidth $\sim 100 \text{ nm}$) and becomes more intense after lowering the temperature to 77 K (figure 3(c)). A quantitative comparison of this signature between different temperatures and different iodine concentrations is not possible due to the sample inhomogeneity, which lead to a varying contribution of the feature around 425 nm across the studied thin films. Moreover, the intensity of the signature decreased after longer illumination with the laser. Nevertheless, a clear trend towards higher intensities at lower temperature and higher iodine concentration is observed. In the data recorded for the $(\text{BA})_4\text{AgBiBr}_4\text{I}_4$ sample (lilac line), the intensity of this peak at low temperature becomes almost 10 times higher than

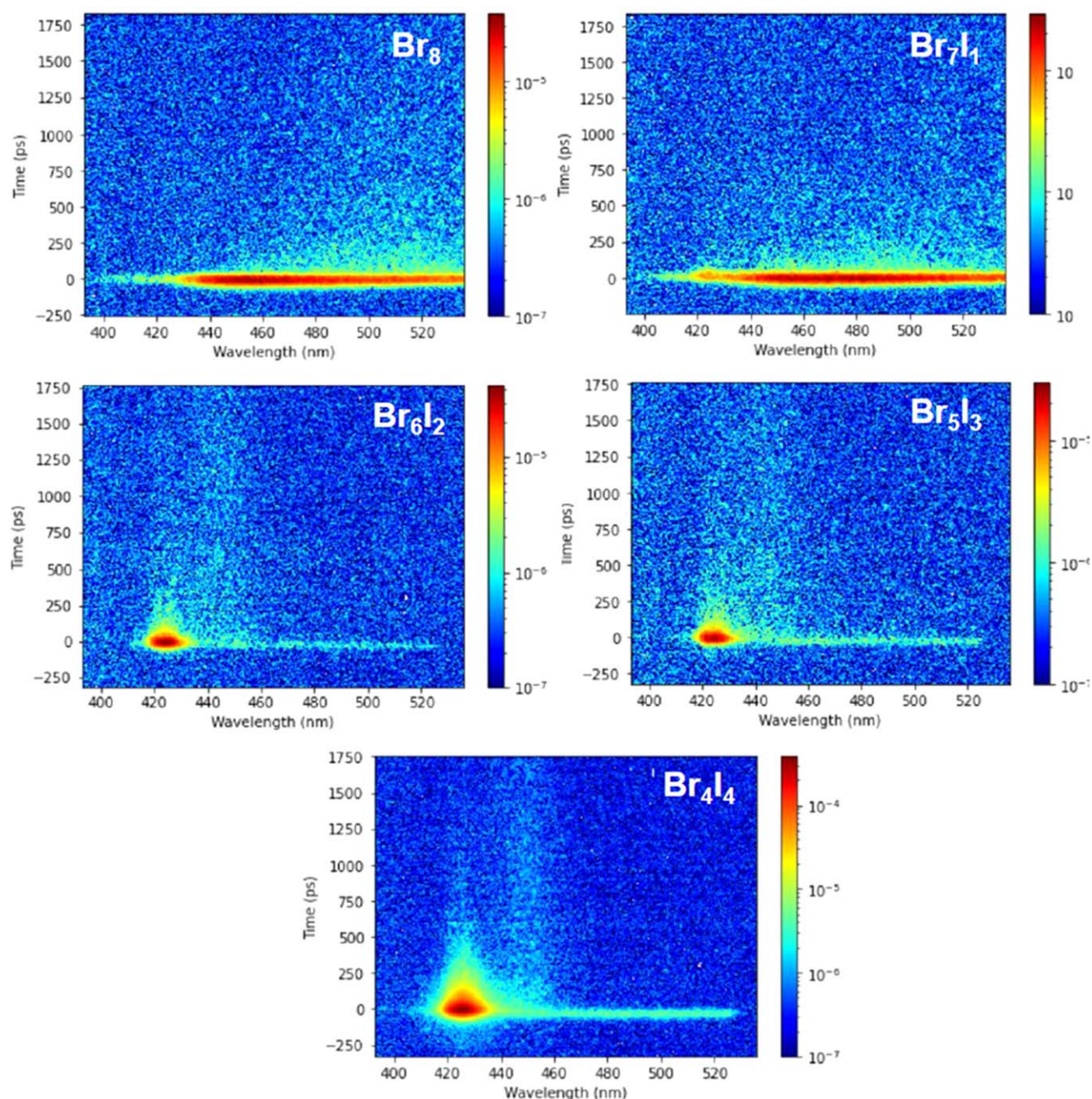


Figure 4. PL decays for the $(\text{BA})_4\text{AgBiBr}_{8-x}\text{I}_x$ ($x = 0, 1, 2, 3, 4$) thin films measured at 77 K ($\lambda_{\text{exc}} = 380$ nm, $E_{\text{exc}} = 3.26$ eV).

in $(\text{BA})_4\text{AgBiBr}_5\text{I}_3$ and $(\text{BA})_4\text{AgBiBr}_6\text{I}_2$ (green and blue line) and indicates strong emission from a presumable free exciton [15], which to the best of our knowledge was never seen before in this type of double perovskites. In this spectrum, a minor contribution at longer wavelengths coming from the trap-mediated recombination typical of the pure bromide system can also be recognized (see figure 3(a)).

We further examined the PL decays of the thin films at 77 K: figure 4 reports three dimensional maps of the PL wavelength/PL decay time/PL intensity correlation, from which it can be qualitatively inferred that the emergence of the pure excitonic emission give rise to longer PL lifetimes, the longest ones clearly evident in the $(\text{BA})_4\text{AgBiBr}_4\text{I}_4$

sample. A more precise quantification of the PL decay is given in the TR-PL spectra in figure S4, in which a fitting has been carried out: typically, two contributions are present, a short one on the order of 20 ps and a longer one between 100 and 250 ps, with the longest time constant coming from some longer-lived emission of the broad signature for the $(\text{BA})_4\text{AgBiBr}_8$ and $(\text{BA})_4\text{AgBiBr}_7\text{I}_1$ samples and from the feature at 425 nm in the other samples. An even shorter contribution emerging from the broad emission peaking around 470 nm could not be fit adequately, as it decayed within the instrument response time. Such a short decay could originate from a high number of non-radiative decay channels introduced by defects. The longer PL decay of the 425 nm

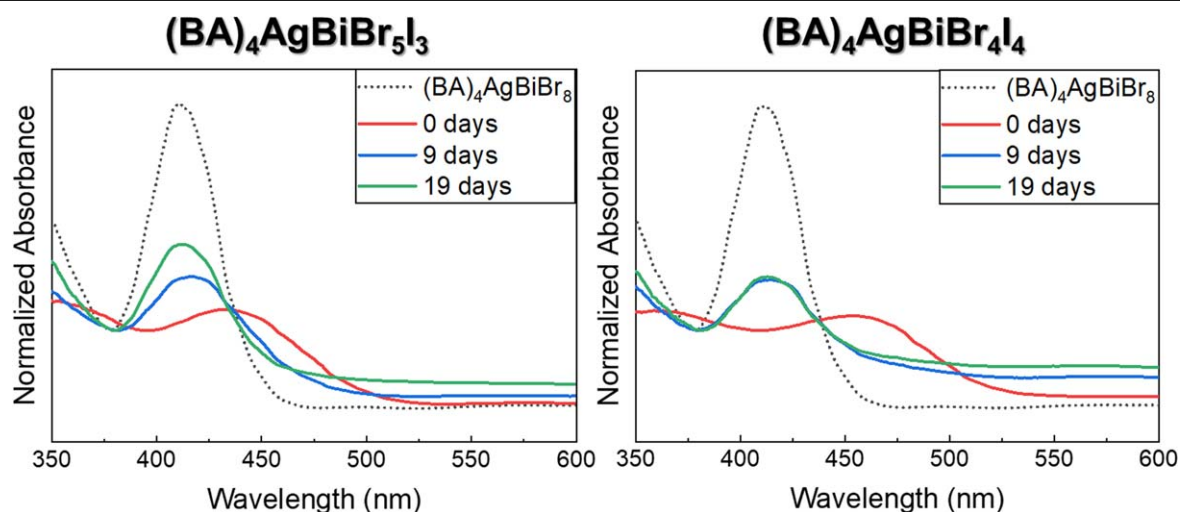


Figure 5. UV–visible absorption spectra for unencapsulated $(\text{BA})_4\text{AgBiBr}_5\text{I}_3$ and $(\text{BA})_4\text{AgBiBr}_4\text{I}_4$ thin films at different times during progressive ageing indoor at 60% relative humidity. The spectrum of the as-prepared $(\text{BA})_4\text{AgBiBr}_8$ thin film is also reported for the sake of comparison.

emission on the other hand indicates the presence of domains with a considerably lower defect density (much brighter, but small in volume, so that they do not appear clearly in absorption and in GIXRD), in which photogenerated excitons or charges can travel for relatively long distances across the inorganic lattice before they recombine radiatively or non-radiatively [31]. A similar scenario might prospect improved photocurrent generation in the system, once better control over these low-defects density domains is achieved, which would be beneficial for photovoltaic applications.

To examine how iodide doping affects the electronic structure of the perovskite and to provide a basis for an appropriate choice of contact materials, we performed KPFM analysis on thin films (figure S6(b)) and compared the perovskite's work function (WF) at varying degrees of iodide content ($x = 0, 1, 2, 4$, figure S6(c)). While the pristine perovskite ($x = 0$) showed a WF of ~ 4.95 eV (see figure S7(c)), an upward shift to ~ 4.80 eV was detected when a small amount of iodide was incorporated ($x = 1$). The WF was shifted even further for the sample with the highest iodide content ($x = 4$), but showed a broadened distribution with a maximum at ~ 4.66 eV and a shoulder at ~ 4.60 eV. This can be explained by an inhomogeneous distribution of iodide across the perovskite surface and/or by an inhomogeneous orientation of the perovskite crystals relative to the substrate, which can lead to differently strong interactions of the tip with monolayer edges. Such differences in orientation were detected in the AFM images in figure S6(a), speaking in favor of at least partial relevance of this explanation. Interestingly, for $x = 2$, topologically homogeneous areas were seen in AFM that showed spots of ~ 500 nm diameter with significantly lowered WF. These result in a broad WF distribution in this sample, with a maximum at the same energy as the undoped pure bromide perovskite and another weaker local maximum at ~ 4.57 eV, a similar energy as the aforementioned shoulder of $(\text{BA})_4\text{AgBiBr}_4\text{I}_4$. We, therefore, conclude that for $x = 2$ a separation of bromide- and iodide-rich phases might have an

influence, whereas iodide is homogeneously distributed even at the surface at $x = 1$. The WF of 4.95 eV determined in the present series for $(\text{BA})_4\text{AgBiBr}_8$ ($x = 0$) significantly deviates from a previously reported value of 4.42 eV [13]. This difference was caused by characteristically different ways of film preparation. When measuring the WF of a thin film obtained from hydrothermally pre-synthesized $(\text{BA})_4\text{AgBiBr}_8$ subsequently dissolved in DMF for spin coating, as in [13], as part of the present series, we confirmed the previously reported WF for such film (see figure S7). Since both $(\text{BA})_4\text{AgBiBr}_8$ films show similar morphology, we assign this difference in WF to differences in surface termination when the metal halide and butylammonium halide precursors are directly dissolved in DMF and casted in the present series as opposed to direct precipitation from $(\text{BA})_4\text{AgBiBr}_8$ crystalline precursors as in [13]. Good opportunities of tuning the contact formation with charge extraction layers by appropriate surface termination are, thereby, indicated.

To evaluate the environmental stability of the mixed iodide-bromide 2D monolayer Ag–Bi perovskite thin films, we exposed the two samples with the more pronounced red shift of the absorption edge, namely $(\text{BA})_4\text{AgBiBr}_5\text{I}_3$ and $(\text{BA})_4\text{AgBiBr}_4\text{I}_4$, to prolonged ageing. The shelf-life test was carried out by maintaining the films for a maximum of 19 days in air at a relative humidity of 60% under standard day/night illumination conditions on a bench within the laboratory (no coverage) and measuring the absorption spectra after 9 and 19 days. The results are shown in figure 5: the spectra for both the samples appear to regain the features of the pure bromide reference compound (shown as dotted line in the figures for comparison), although they do not recover completely the same intensity in the excitonic transition.

We believe that what we observe here is a progressive loss of iodide most likely in the form of volatile I_2 [20, 32] (easily undergoing sublimation in standard environmental conditions) and consequent rearrangement of the crystal lattice, as arguable from the top-view SEM images reported in figure S9. This process is undoubtedly accelerated in the

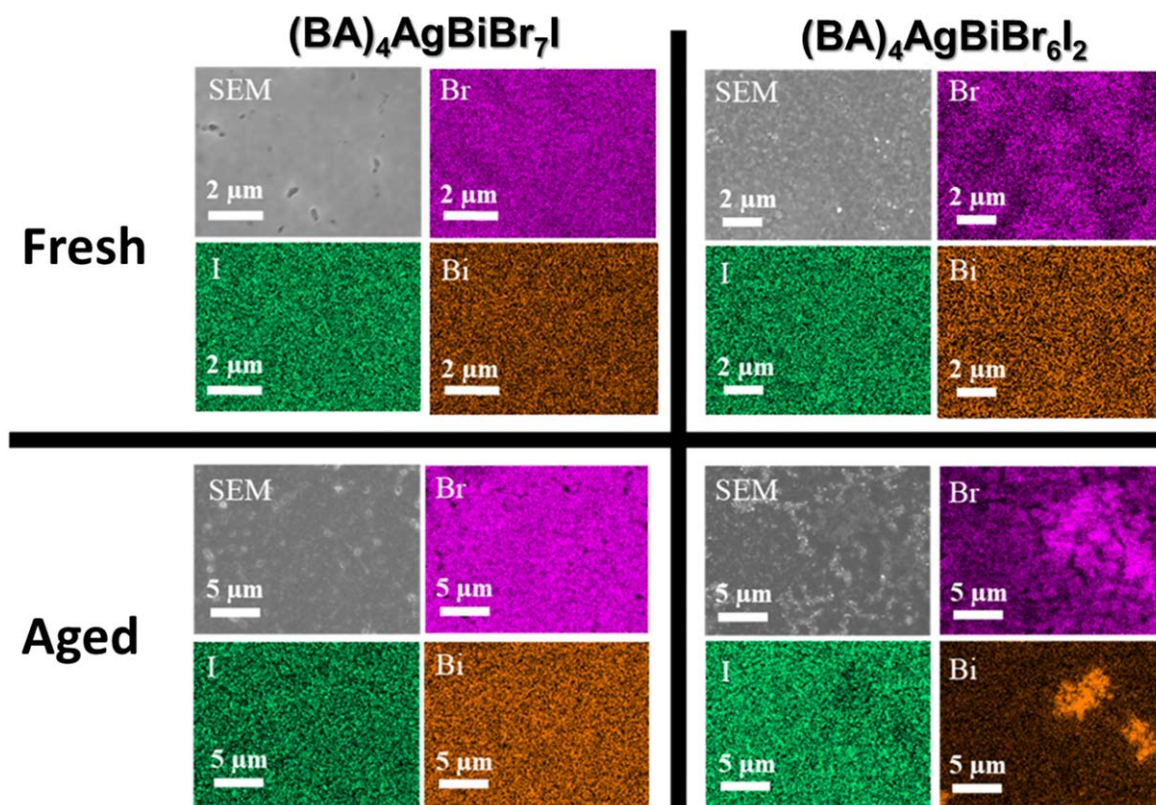


Figure 6. Elemental maps of bromide, iodide and bismuth distribution for $(\text{BA})_4\text{AgBiBr}_7\text{I}$ (left) and $(\text{BA})_4\text{AgBiBr}_6\text{I}_2$ (right) thin films that were freshly prepared (top) and underwent prolonged ageing (bottom) as obtained by EDX. SEM images of the measured areas are depicted in the respective top left corner for the sake of clarity.

presence of light, heat and/or humidity, which trigger decomposition by generating surface defects that promote iodine release [32]. The relatively thin and pinhole-rich films for these two bromide-compositions (see figure 1(c)), likely forming as the result of the higher dilution in the precursor solutions that we were forced to employ, offers undoubtedly more surface sites for the occurrence of similar degradation pathways. The influence of light in this process is further suggested by the progressive disappearance of the free exciton PL signal under prolonged laser excitation (1–2 min times, data not shown).

The iodide loss can be indeed verified from samples with x values up to 2 from EDX analysis (see table S2). Additionally, GIXRD measurements on aged samples (see figures S2(c), (d)) show that in thin films with high iodide content ($x = 2, 3, 4$) a reflex at 12.0° , that could not be observed in freshly prepared samples, appears and is particularly intense for the $(\text{BA})_4\text{AgBiBr}_4\text{I}_4$ aged sample. Although elemental maps measured by EDX (figure 6) show agglomerations of bismuth and bromide in the aged $(\text{BA})_4\text{AgBiBr}_6\text{I}_2$ sample, this new XRD reflex could not be assigned to BiBr_3 or to any other used precursor. Elemental maps further show a homogeneous distribution of silver (see figure S10) for freshly prepared as well as aged samples, while the iodide content decreases slightly at locations of increased bismuth and bromide co-localization in the aged $(\text{BA})_4\text{AgBiBr}_6\text{I}_2$ thin film. On the other hand, $(\text{BA})_4\text{AgBiBr}_7\text{I}$ thin film presents a homogeneous distribution for all elements, in freshly prepared

samples as well as in degraded samples. Therefore, we assume that the aforementioned newly appearing reflex has to be assigned to a yet unknown Bi- and Br-rich side phase which forms upon degradation.

4. Conclusion

In this work we report, to the best of our knowledge, the first study on the production of mixed halide thin films of a 2D monolayer silver-bismuth double perovskite and study their optical properties, aiming at providing first hints on their potential utilization as light absorber in the future generation of low-cost, environmentally friendly photovoltaic devices to power the IoT. We unravel very interesting insights from the study of these double perovskite materials, which could represent a valuable alternative to the use of the mono-halide counterparts, which particularly for the case of pure iodides, having the most promising expected bandgap, have only very rarely been isolated and characterized, due to a lack of lattice stability [20]. For increasing proportions of iodide alloying in a reference bromide phase, we observe a progressive bathochromic shift of the absorption edge which brings to cover an always larger part of the typical emission spectrum of a WLED lamp. We also provide evidence for the emergence of domains with a higher radiative yield likely due to lower amounts of defects, which could have a positive impact on the generation of free charges following light absorption, to be

collected as a photocurrent in suitably arranged photovoltaic architectures.

Since the environmental stability of these materials under prolonged exposure to light and air humidity results still very limited, we envisage the possibility to further boost the robustness of these systems by performing organic layer engineering: in the present preliminary study we made use of a very simple alkylammonium cation, but in our previous work we have already demonstrated that in the pure bromide structure the use of an aromatic cation brings to a stabilization of the lattice through the establishment of further van der Waals interactions within the organic double layer [13] and it has also been reported for mixed halide phases of lead-based perovskites by other groups [18, 26].

A limitation that still has to be faced for prospecting good efficiency in PV devices regards the obtainment of a preferential vertical orientation with respect to a substrate, which would favor the removal of the photo-generated free charges in the 2D perovskite by means of adjacent charge extracting layers. To allow access to this crystalline configuration, different methods have been reported to be employed during thin film processing, such as the hot casting method and the additive assisted crystallization [33], which should be thoroughly explored in future work. As in this study we have revealed first hints of the tendency towards a vertical arrangement of the most iodide-enriched thin films, we can guess that we are moving in the right direction to enable an optimal morphology for this scope after further optimization of the layer casting method. All these further studies will be very useful to allow the actual future utilization of these highly promising material platforms in sustainable solar cells or other optoelectronic devices.

Acknowledgments

T G would like to acknowledge financial support of the European commission through the H2020 FET-PROACTIVE-EIC-07-2020 project LIGHT-CAP (project number 101017821) and of the Deutsche Forschungsgemeinschaft (DFG, German Research Foundation) through the project GA 3052/1-1. T G also thanks the ENSEMBLE3-Centre of Excellence for nanophotonics, advanced materials and novel crystal growth-based technologies project (GA No. MAB/2020/14) carried out within the International Research Agendas programme of the Foundation for Polish Science co-financed by the European Union under the European Regional Development Fund and the European Union's Horizon 2020 research and innovation programme Teaming for Excellence (GA. No. 857543) for support of this work. M G thanks Prof Martin Koch for his support and access to experimental equipment.

Data availability statement

All data that support the findings of this study are included within the article (and any supplementary files).

ORCID iDs

Derck Schlettwein  <https://orcid.org/0000-0002-3446-196X>
Teresa Gatti  <https://orcid.org/0000-0001-5343-8055>

References

- [1] Li J, Cao H-L, Jiao W-B, Wang Q, Wei M, Cantone I, Lü J and Abate A 2020 Biological impact of lead from halide perovskites reveals the risk of introducing a safe threshold *Nat. Commun.* **11** 310
- [2] Ju M-G, Dai J, Ma L and Zeng X C 2017 Lead-free mixed tin and germanium perovskites for photovoltaic application *J. Am. Chem. Soc.* **139** 8038–43
- [3] Chiara R, Morana M and Malavasi L 2021 Germanium-based halide perovskites: materials, properties, and applications *Chempluschem* **86** 879–88
- [4] Pecunia V, Occhipinti L G, Chakraborty A, Pan Y and Peng Y 2020 Lead-free halide perovskite photovoltaics: challenges, open questions, and opportunities *APL Mater.* **8** 100901
- [5] Jin Z, Zhang Z, Xiu J, Song H, Gatti T and He Z 2020 A critical review on bismuth and antimony halide based perovskites and their derivatives for photovoltaic applications: recent advances and challenges *J. Mater. Chem. A* **8** 16166–88
- [6] Peng Y, Huq T N, Mei J, Portilla L, Jagt R A, Occhipinti L G, MacManus-Driscoll J L, Hoyer R L Z and Pecunia V 2021 Lead-free perovskite-inspired absorbers for indoor photovoltaics *Adv. Energy Mater.* **11** 2002761
- [7] Pecunia V, Occhipinti L G and Hoyer R L Z 2021 Emerging indoor photovoltaic technologies for sustainable internet of things *Adv. Energy Mater.* **11** 2100698
- [8] Longo G, Mahesh S, Buizza L R V, Wright A D, Ramadan A J, Abdi-Jalebi M, Nayak P K, Herz L M and Snaith H J 2020 Understanding the performance limiting factors of Cs₂AgBiBr₆ double-perovskite solar cells *ACS Energy Lett.* **5** 2200–7
- [9] Schmitz F *et al* 2020 Lanthanide-induced photoluminescence in lead-free Cs₂AgBiBr₆ bulk perovskite: insights from optical and theoretical investigations *J. Phys. Chem. Lett.* **11** 8893–900
- [10] Schade L *et al* 2019 Structural and optical properties of Cs₂AgBiBr₆ double perovskite *ACS Energy Lett.* **4** 299–305
- [11] Connor B A, Leppert L, Smith M D, Neaton J B and Karunadasa H I 2018 Layered halide double perovskites: dimensional reduction of Cs₂AgBiBr₆ *J. Am. Chem. Soc.* **140** 5235–40
- [12] Jana M K, Janke S M, Dirkes D J, Dovletgeldi S, Liu C, Qin X, Gundogdu K, You W, Blum V and Mitzi D B 2019 Direct-bandgap 2D silver–bismuth iodide double perovskite: the structure-directing influence of an oligothiophene spacer cation *J. Am. Chem. Soc.* **141** 7955–64
- [13] Schmitz F *et al* 2021 Large cation engineering in two-dimensional silver–bismuth bromide double perovskites *Chem. Mater.* **33** 4688–700
- [14] Zheng Y, Niu T, Ran X, Qiu J, Li B, Xia Y, Chen Y and Huang W 2019 Unique characteristics of 2D Ruddlesden–Popper (2DRP) perovskite for future photovoltaic application *J. Mater. Chem. A* **7** 13860–72
- [15] Righetto M, Giovanni D, Lim S S and Sum T C 2021 The photophysics of Ruddlesden–Popper perovskites: a tale of energy, charges, and spins *Appl. Phys. Rev.* **8** 11318
- [16] Righetto M, Meggiolaro D, Rizzo A, Sorrentino R, He Z, Meneghesso G, Sum T C, Gatti T and Lamberti F 2020 Coupling halide perovskites with different materials: from

- doping to nanocomposites, beyond photovoltaics *Prog. Mater. Sci.* **110** 100639
- [17] Li C, Wei J, Sato M, Koike H, Xie Z-Z, Li Y-Q, Kanai K, Kera S, Ueno N and Tang J-X 2016 Halide-substituted electronic properties of organometal halide perovskite films: direct and inverse photoemission studies *ACS Appl. Mater. Interfaces* **8** 11526–31
- [18] Zanetta A *et al* 2021 Manipulating color emission in 2D hybrid perovskites by fine tuning halide segregation: a transparent green emitter *Adv. Mater.* **34** 2105942
- [19] Bonomi S, Galinetto P, Patrini M, Romani L and Malavasi L 2021 Optical and structural property tuning in physical vapor deposited bismuth halides Cs₃Bi₂(I_{1-x}Br_x)₉ ($0 \leq x \leq 1$) *Inorg. Chem.* **60** 14142–50
- [20] Vishnoi P, Seshadri R and Cheetham A K 2021 Why are double perovskite iodides so rare? *J. Phys. Chem. C* **125** 11756–64
- [21] Fairley N *et al* 2021 Systematic and collaborative approach to problem solving using x-ray photoelectron spectroscopy *Appl. Surf. Sci. Adv.* **5** 100112
- [22] Zarick H F, Soetan N, Erwin W R and Bardhan R 2018 Mixed halide hybrid perovskites: a paradigm shift in photovoltaics *J. Mater. Chem. A* **6** 5507–37
- [23] Chen Z, Brocks G, Tao S and Bobbert P A 2021 Unified theory for light-induced halide segregation in mixed halide perovskites *Nat. Commun.* **12** 2687
- [24] Knight A J, Borchert J, Oliver R D J, Patel J B, Radaelli P G, Snaith H J, Johnston M B and Herz L M 2021 Halide segregation in mixed-halide perovskites: influence of a-site cations *ACS Energy Lett.* **6** 799–808
- [25] Cho J, Mathew P S, DuBose J T and Kamat P V 2021 Photoinduced halide segregation in Ruddlesden–Popper 2D mixed halide perovskite films *Adv. Mater.* **33** 2105585
- [26] Mathew P S, DuBose J T, Cho J and Kamat P V 2021 Spacer cations dictate photoinduced phase segregation in 2D mixed halide perovskites *ACS Energy Lett.* **6** 2499–501
- [27] Li X, Traoré B, Kepenekian M, Li L, Stoumpos C C, Guo P, Even J, Katan C and Kanatzidis M G 2021 Bismuth/silver-based two-dimensional iodide double and one-dimensional Bi perovskites: interplay between structural and electronic dimensions *Chem. Mater.* **33** 6206–16
- [28] Bi L-Y, Hu Y-Q, Li M-Q, Hu T-L, Zhang H-L, Yin X-T, Que W-X, Lassoued M S and Zheng Y-Z 2019 Two-dimensional lead-free iodide-based hybrid double perovskites: crystal growth, thin-film preparation and photocurrent responses *J. Mater. Chem. A* **7** 19662–7
- [29] Giovanni D, Ramesh S, Righetto M, Melvin Lim J W, Zhang Q, Wang Y, Ye S, Xu Q, Mathews N and Sum T C 2021 The physics of interlayer exciton delocalization in Ruddlesden–Popper lead halide perovskites *Nano Lett.* **21** 405–13
- [30] Li S, Luo J, Liu J and Tang J 2019 Self-trapped excitons in all-inorganic Halide Perovskites: fundamentals, status, and potential applications *J. Phys. Chem. Lett.* **10** 1999–2007
- [31] Liang M *et al* 2021 Free carriers versus self-trapped excitons at different facets of Ruddlesden–Popper two-dimensional lead halide perovskite single crystals *J. Phys. Chem. Lett.* **12** 4965–71
- [32] Wu W-Q, Rudd P N, Ni Z, Van Brackle C H, Wei H, Wang Q, Ecker B R, Gao Y and Huang J 2020 Reducing surface halide deficiency for efficient and stable iodide-based perovskite solar cells *J. Am. Chem. Soc.* **142** 3989–96
- [33] Zhao X, Liu T and Loo Y-L 2022 Advancing 2D perovskites for efficient and stable solar cells: challenges and opportunities *Adv. Mater.* **34** 2105849